

Relaxations and bonding mechanism in $\text{Hg}_{1-x}\text{Cd}_x\text{Te}$ with mercury vacancy defect: First-principles study

L. Z. Sun,^{1,2} Xiaoshuang Chen,^{1,*} Y. L. Sun,¹ X. H. Zhou,¹ Zh. J. Quan,¹ He Duan,¹ and Wei Lu^{1,†}

¹National Laboratory for Infrared Physics, Shanghai Institute of Technical Physics, Chinese Academy of Science, 200083 Shanghai, China

²Faculty of Materials and Optoelectronic Physics, Xiangtan University, 411105 Hunan, China

(Received 27 October 2004; revised manuscript received 13 April 2006; published 16 May 2006)

The structural and electronic properties of the mercury vacancy defect in $\text{Hg}_{1-x}\text{Cd}_x\text{Te}$ have been studied by combining the full-potential linear augmented plane wave and plane-wave pseudopotential method based on the density functional theory. Structural relaxation, local charge density, and on-site and partial densities of states are computed to investigate the effects of the mercury vacancy on the electronic structure. The characteristics of dangling bond rehybridization due to the mercury vacancy are discussed by analysis of the valence charge density and the bonding charge density. We reveal upshift of the energy level for the 5s states of the nearest neighbor tellurium of the defect due to dangling bond rehybridization. The double acceptor levels introduced by the vacancy are determined by the single-particle electron energy calculations and the transition energy levels, which agree well with the experimental results.

DOI: [10.1103/PhysRevB.73.195206](https://doi.org/10.1103/PhysRevB.73.195206)

PACS number(s): 71.55.Gs, 71.20.Nr, 71.15.Pd

I. INTRODUCTION

Mercury cadmium telluride ($\text{Hg}_{1-x}\text{Cd}_x\text{Te}$, MCT) is currently one of the most widely used semiconductor materials for infrared detector arrays. It is well known that structural defects are introduced inevitably in MCT materials either in the process of materials growth or in the process of device fabrication. Point defects are important in controlling carrier concentrations, minority-carrier lifetimes, and noise in $\text{Hg}_{1-x}\text{Cd}_x\text{Te}$.^{1,2} In the simplest terms, the type and concentration of the free carriers can be controlled by the defects that introduce shallow levels in the band gap of $\text{Hg}_{1-x}\text{Cd}_x\text{Te}$, while the minority-carrier lifetimes and noise are controlled by the defects associated with deep levels in the band gap. The importance of native defects in $\text{Hg}_{1-x}\text{Cd}_x\text{Te}$ is undisputed. In many circumstances, the physical properties of $\text{Hg}_{1-x}\text{Cd}_x\text{Te}$ and its dopability are dominated by native point defects.³ Vydyanath⁴ has revealed that most important native defects in $\text{Hg}_{1-x}\text{Cd}_x\text{Te}$ is the double acceptor mercury vacancy. Gold⁵ *et al.* have further pointed out that the mercury vacancy defect in MCT introduces not only a shallow acceptor level but also a deep level at 40% of the band gap. It is known that vacancies play a role in many electrical properties in semiconductors, for example, acting as largely uncontrolled dopants and affecting the electron and hole mobilities.^{6,7} The structural properties are also sensitive to the existence of vacancies,⁸ such as, dislocation formation and propagation, as well as self-diffusion⁹ and diffusion of impurities,^{10,11} depending on the vacancy concentrations. Moreover the vacancy defects are not only formed in the process of materials growth, but also introduced when exposing of the device to a radiation such as electrons,¹² laser,¹³ or some light ion^{14,15} radiations. Such complicated working circumstance dominates the performance of the device. Unfortunately, the experimental evidences on the electronic properties associated with mercury vacancy defects are mainly indirect and depend on their ionization states. The neutral

defects and compensating defects are even more difficult to observe.

Although there are some theoretical studies on the mercury vacancy in MCT materials or in II-VI semiconductors (CdTe , HgTe),¹⁶⁻¹⁹ the characteristic of bonding mechanism around the vacancy, namely, the dangling bond rehybridization, has not been reported as yet, to our knowledge. Defects certainly induce local relaxation on the atomic structure. The relaxation may change the symmetry of the local lattice, disturb the charge distribution in the vicinity of the defect, and modify the positions of the defect energy levels and the corresponding localized states. Recently, Errico^{20,21} *et al.* have revealed the influence of the charge states of the systems on the relaxation procedure and the electronic states. Up to now, there have not been reports on the effect of the mercury vacancy on the induced relaxation procedure because of different charge states and local atomic configurations, and on the dependence of atomic configuration on the mole fraction x in MCT. Since the electronic and structural properties of HgCdTe are considered to originate from vacancies, the understanding of the electronic properties of mercury vacancy in MCT is important to reveal their alloy's behavior.

For these purposes, we have performed the total energy calculations of full potential linear augmented plane wave (FP-LAPW) to systematically investigate the effect of the mercury vacancy defect on the electronic structure, the bonding mechanism accompanying with the dangling bond rehybridization, the relaxation procedure for different charge states in $\text{Hg}_{1-x}\text{Cd}_x\text{Te}$. In this paper, we choose $\text{Hg}_{0.5}\text{Cd}_{0.5}\text{Te}$ as the major prototype system. The reason for choosing such a mole fraction is that the computational results can be compared with that of the thoroughly studied II-VI semiconductors (CdTe and HgTe) to some extent. On the other hand, the results can be easily extrapolated to other mole fraction compositions. Furthermore, the results and conclusions of the calculations on $\text{Hg}_{0.5}\text{Cd}_{0.5}\text{Te}$ are confirmed, and also extended to the other mole fractions by using plane-wave

pseudopotential calculations with larger supercells.

The remainder of the paper is organized as follows. Section II describes our computational methods. The results and discussions are presented in Sec. III. We discuss the relaxation procedure corresponding to different charge states and mole fractions, the bonding mechanism, and the shift of energy states according to the dangling bond rehybridization induced by the mercury vacancy. The relationship between formation energy and the mole fractions of MCT is also calculated and discussed. Section IV gives a brief summary of this work.

II. COMPUTATIONAL PROCEDURE

The density functional theory²² calculations are performed using the FP-LAPW method implemented in the WIEN2K package.²³ We adopt Perdew-Burke-Ernzerhof functional²⁴ to describe the exchange-correlation interaction. We consider a $2 \times 2 \times 2$ supercell (SC) with totally 64 atoms, consisting of eight quasi-zinc-blende crystal structure of unit cells $\text{Hg}_{0.5}\text{Cd}_{0.5}\text{Te}$ (each unit cell contains eight atoms including four Te atoms, two Hg atoms, and two Cd atoms). In the SC model, one of the 16 mercury atoms on the lattice site (0.5, 0.5, 0.5) of SC is replaced by a vacancy. A $2 \times 2 \times 1$ SC with 32 atoms of no vacancy has been chosen as reference system for comparison purpose, and the computational parameters are set to be the same as the vacancy case. In order to ensure well convergence, the muffin-tin (MT) radius and the number of k -points for generating the final results have been carefully chosen after optimization. The states treated as valence are $\text{Hg}(5d^{10}6s^2)$, $\text{Cd}(4d^{10}5s^2)$, and $\text{Te}(5s^25p^4)$. The muffin-tin radii are chosen to be 2.60 atomic units (a.u.) for all the three kinds atoms. A satisfactory self-consistent convergence has been achieved by considering a number of FP-LAPW basis functions up to $R_{\text{MT}}K_{\text{max}}=6.0$ for the 64-atom SC and $R_{\text{MT}}K_{\text{max}}=7.0$ for 32-atom SC. The K_{max} is the maximum value of the plane-wave vector that determines the so-called energy cutoff for the plane-wave expansion. The self-consistent iteration is considered to be converged when both the total energy and the total charge in the atomic sphere are stable within 10^{-4} eV per unit cell and 10^{-4} electron charges per atom, respectively. The localized levels are deduced from the calculations of the single-electron energy levels at Γ point and are aligned using the energy levels of core electrons. The relaxation procedures are conducted following the damped Newton dynamic schemes.^{25–27} The criterion of the forces convergence for all atoms is set below 0.05 eV/Å. The relativistic effect of spin-orbit (SO) coupling is also included.

To confirm the results on the supercell of 64 atoms using FP-LAPW methods and extend the conclusions to the other mole fractions of MCT, the plane-wave pseudopotential code Vienna *ab initio* simulation package^{28,29} (VASP) is also used in this paper. In the VASP calculations, the core-electron interaction is modeled by the ultrasoft pseudopotentials,³⁰ which can yield reasonably precise results with relatively low cutoff energy. Thus, it is possible to deal with the larger supercell. In the present paper, supercells with 256 and 512 atoms have been chosen. The plane-wave cutoff energy is

chosen as 300 eV, the standard ultrasoft pseudopotentials from the VASP package are employed for all the cases, and the Brillouin zone is sampled by using $5 \times 5 \times 5$ and $3 \times 3 \times 3$ Monkhorst-Pack grid for 256-atom and 512-atom supercells, respectively. The energy convergent criterion is 1×10^{-4} eV per unit cell, and forces on all relaxed atoms are less than 0.01 eV/Å.

It is well known that the local density approximation calculations typically underestimate the band gap of a semiconductor and is not able to give the absolute positions of the acceptors accompanying with the Hg vacancy defect very accurately. The emphasis here have been placed on the analysis of the defect formation energy and the transition energy levels. At temperature of zero Kelvin, the defect formation energy in a given charge state q is given by^{3,31}

$$\Delta H_f(V_{\text{Hg}}, q) = E(V_{\text{Hg}}, q) + E(\text{Hg}) - E(\text{MCT}) + qE_{\text{VBM}} + qE_{\text{F}} + \mu_{\text{Hg}}, \quad (1)$$

where $\Delta H_f(V_{\text{Hg}}, q)$ is the formation energy for a supercell containing the vacancy defect in charge state q . $E(V_{\text{Hg}}, q)$ and $E(\text{MCT})$ are the total energies for the supercell containing the mercury vacancy defect in charge state q and the same size supercell without defect, respectively. It is well known that MCT is a pseudobinary alloy, which means the two types of cations occupy randomly the cation sites. Different local concentrations of cations are accompanied with the disordered effect in MCT. Within a simple model, the disordered system can be treated approximately as the mixture of MCT with different mole fractions. Just as Shih *et al.* have pointed out,³² the valence band maximum (VBM) becomes lower as the mole fraction x becomes larger. Thus, the reference of electronic Fermi energy E_{F} in the MCT alloy is chosen to the VBM of CdTe in the present work. $E(\text{Hg})$ and μ_{Hg} are the total energy of Hg referencing to element and the chemical potential of Hg, respectively. Equation (1) indicates that the formation energy with Hg vacancy defect, $\Delta H_f(V_{\text{Hg}}, q)$, is a function of the E_{F} and the chemical potential of Hg, μ_{Hg} . The defect transition energy level $\varepsilon_a(q/q')$ is the Fermi energy E_{F} in Eq. (1), at which the formation energy $\Delta H_f(V_{\text{Hg}}, q)$ of vacancy defect and charge q is equal to that of another charge q' . The formation energy and transition energy levels of MCT with cation vacancy defect are calculated by projector augmented wave (PAW) method for the supercell of 64 atoms. For the systems with charged defect, a uniform background charge is added to keep the global charge neutrality of the periodic supercell. The total energy of the systems with charged defect has been corrected for the interaction of the charged defect with the compensating background and its periodic images.³³ In the 64-atom supercell due to the finite cell size, basis set, and k -point sampling used, the error bars are about 0.2 and 0.1 eV for the calculated formation energy and transition energy, respectively.

III. RESULTS AND DISCUSSION

A. Structural relaxation

The appearance of cation vacancy defects induces the structural relaxation of the host and modifies the electronic

structure of the system. Before relaxation of atomic structures, from the calculated total energy versus five different volumes around the lattice constants given by Vegard's law, the equilibrium volumes have been obtained for MCT systems with and without vacancy defect, respectively. All the calculated values are fitted to the Murnaghan equation of state.³⁴ In comparison with the experimental results, the computed bond lengths of $R(\text{Te}-\text{Cd})$ and $R(\text{Te}-\text{Hg})$ are about 1% larger than that of experimental results of CdTe and HgTe. Geometry optimizations reveal that the cation vacancy defects lead to inward relaxation of the nearest-neighbor (NN) anions, in agreement with the previous studies.⁸ Meanwhile, the bond lengths between the NN Te atoms and the next-nearest-neighbor (NNN) cations are also reduced. The result indicates that the inward relaxation of the NNN cations is larger than that of NN anions. In order to find out the reason of the NN Te inward relaxation in MCT caused by cation vacancy defects, the valence charge density and the bonding charge density have been calculated. The bonding charge density is defined as the difference between the total charge density in the solid and the superpositions of neutral atomic charge densities placed at atomic sites; i.e.,

$$\Delta\rho(r) = \rho_{\text{solid}}(r) - \sum_{\alpha} \rho_{\alpha}(r - r_{\alpha}). \quad (2)$$

Therefore, the bonding charge density represents the net charge redistribution as atoms are brought together to form the crystal. The dangling bond rehybridization³⁵ induced by the vacancy defect also can be revealed clearly by the bonding charge density. The calculated valence charge density and the bonding charge density of $\text{Hg}_{0.5}\text{Cd}_{0.5}\text{Te}$ in the (110) plane, containing the mercury vacancy site and the NNN Cd sites are shown in the Fig. 1. The charge accumulation on the vacancy site, and between the NN Te site and the vacancy site can be observed. Namely, the mercury vacancy becomes a negative charge center accompanying with the dangling bond rehybridization of the NN Te atoms. The Coulomb attractive potential between the negatively charged vacancy site and the ions makes the NN anions and the NNN cations move inward. The charge statistics shows that all the four NN Te and 12 NNN cations around the mercury vacancy have their charges to transfer out of the MT sphere by comparing with the total charge of the same MT sphere in MCT without the vacancy defect. There are about 0.1 electrons departing from the NN tellurium MT sphere, implying that there are more than 0.1 electrons accumulating at the vacancy site. In order to confirm the results of the FP-LAPW calculations on the supercell with 64 atoms, larger supercells have been used, such as supercells with 256 atoms and 512 atoms, respectively. The structural relaxations are conducted by using PAW method implemented in VASP. As shown in Table I, PAW calculations with 512-atom supercells give the same relaxation trend of NN Te and NNN cations as that of the FP-LAPW calculations. The numerical results using two different methods demonstrate the inward relaxations of NN Te and NNN cations. Relatively larger radial relaxation of the PAW calculations comes from relatively small force criterion by comparison with that of FP-LAPW calculations. Considering the large calculated time consuming, full relax-

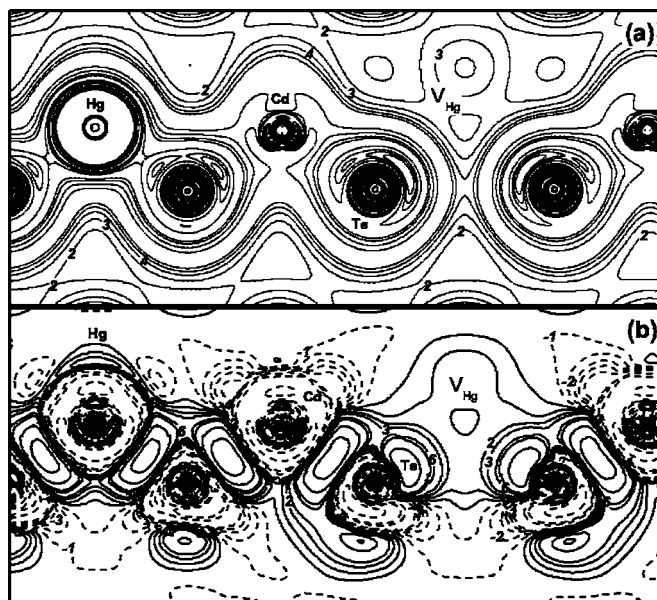


FIG. 1. The valence charge density (a) and the bonding charge density (b) of $\text{Hg}_{0.5}\text{Cd}_{0.5}\text{Te}$ with Hg vacancy in the plane (110), including the NNN Cd. The contour step size is $0.8 \times 10^{-3} e/(\text{a.u.})^3$ for the valence charge density (a) and $0.2 \times 10^{-3} e/(\text{a.u.})^3$ for the bonding-charge density (b). V_{Hg} indicates the mercury vacancy lattice site.

ation of atomic positions is used in PAW calculations, while symmetry constraint is applied in FP-LAPW calculations. Approximately linear relationship between the inward relaxation of the NN Te atoms and the mole fractions of MCT is shown in Fig. 2. Namely, the inward relaxations of the NN Te atoms become smaller as the mole fractions become larger.

The density of states (DOS) calculated for the neutral vacancy defect V_{Hg}^0 is shown in the Fig. 3. One can see that the Fermi level does not lie within the band gap region, while it locates within the valence band. From the DOS shown in Fig. 3(b), the integration from the Fermi level to the conduction band bottom accommodates two electrons. Accordingly,

TABLE I. The relaxing results of the nearest-neighbor (NN) Te atoms and the next-nearest-neighbors (NNN) cations for the system with different charge states. $\Delta d(V_{\text{Hg}}-\text{Te}^1)$, $\Delta d(\text{Te}^1-\text{Cd}^2)$, and $\Delta d(\text{Te}^1-\text{Hg}^2)$ are the relaxations (in Å) of the NN Te atoms relative to the vacancy site, and between the NN Te and NNN cations, respectively. Minus means inward relaxation.

	$\Delta d(V_{\text{Hg}}-\text{Te}^1)$	$\Delta d(\text{Te}^1-\text{Cd}^2)$	$\Delta d(\text{Te}^1-\text{Hg}^2)$
V^0	-0.09	-0.04	-0.03
V^{-1}	-0.11	-0.05	-0.04
V^{-2}	-0.10	-0.05	-0.04
HgTe (PAW)	-0.37	—	-0.07
0.25 (PAW)	-0.34	-0.07	-0.06
0.5 (PAW)	-0.33	-0.06	-0.07
0.75 (PAW)	-0.29	-0.07	—
CdTe (PAW)	-0.13	-0.06	—

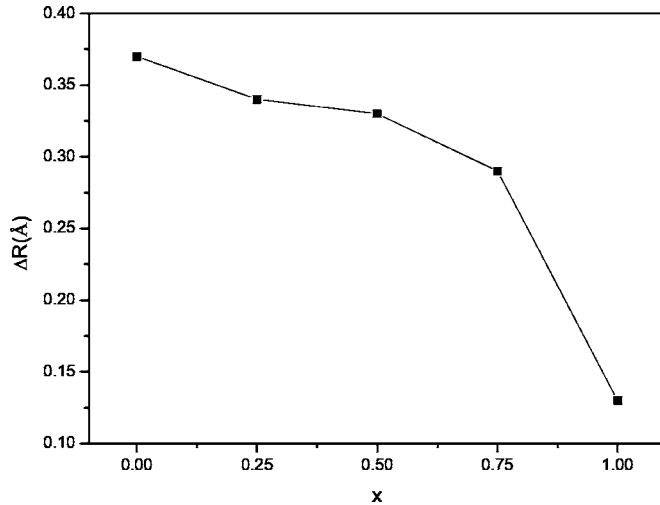


FIG. 2. The relationship between the inward relaxations of the NN Te and the mole fraction of MCT.

these empty states are identified as the double acceptor levels, and the details will be discussed below. In the present work, we perform the calculations for three systems with different charged states, corresponding with three different situations: (i) V_{Hg}^0 , neutral defect state, an extremely pure crystal at low temperatures; (ii) V_{Hg}^{-1} , one charged acceptor state, providing one electron to the double acceptor state of the system; and (iii) V_{Hg}^{-2} , double charged acceptor state. In case (i), we use the 64-atom supercell described in Sec. II. However, in the studies of cases (ii) and (iii), with the same 64-atom supercell, we perform self-consistent calculations with one and two additional electrons to the supercell, respectively. Finally, the self-consistent FP-LAPW calculations are performed as follows:

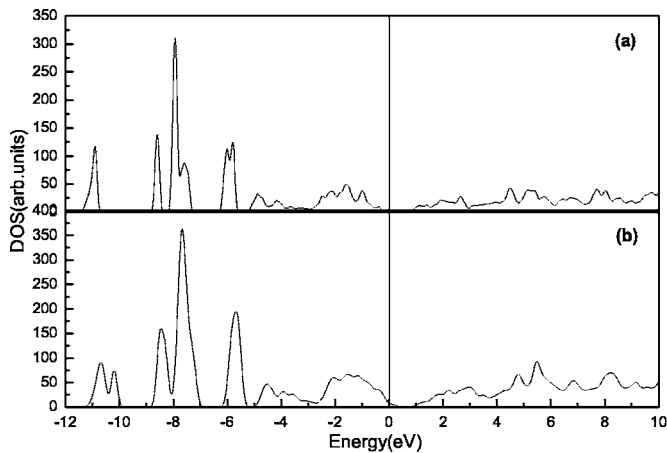


FIG. 3. The total density of states in $\text{Hg}_{0.5}\text{Cd}_{0.5}\text{Te}$ without (a) and with (b) Hg vacancy, respectively. Fermi level is set to zero. The following Fermi level in the DOS figures is in the same way.

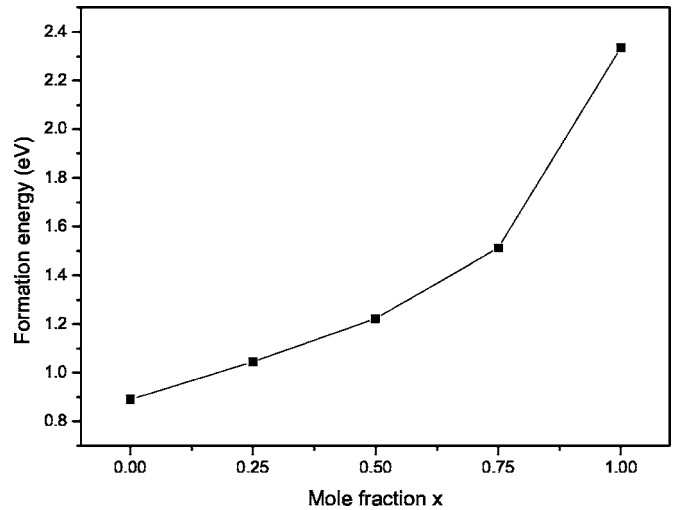
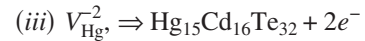


FIG. 4. The calculated formation energies for five mole fractions with cation vacancy defect at neutral charge state ($q=0$) and chemical potential $\mu_{\text{cation}}=0$.



The computational results with different charge states are summarized in the Table I. We find that the inward relaxations of the NN Te for cases (ii) and (iii) are larger than that in case (i). As mentioned above, the rehybridization of the dangling bond around the vacancy site induces the negative charge center to cause the inward relaxation for case (i). In cases (ii) and (iii), the charged states enhance the negative charge center and the Coulomb attractive interaction, thus lead to larger inward relaxation for cases (ii) and (iii) than that of the case (i). Meanwhile, the bond length between the NN Te and NNN cations almost remain the same as that of case (i). The result means that the attractive potential also makes the cations more inward relaxation than that of the case (i).

The relaxation procedure corresponding to different charge states as described above also exists in the other mole fractions and is confirmed by calculating on a larger supercell with the PAW method for all the five mole fractions. The radial relaxations according to different charge states for 512-atom supercell by using the PAW method are in approximate agreement with that of the FP-LAPW method. For the same reason as mentioned above, the magnitude of the radial relaxations using the PAW method is larger than that of LAPW results.

B. Formation energy

The formation energies of the mercury vacancy defect in MCT for four different mole fractions ($x=0, 0.25, 0.5, 0.75$), and the cadmium vacancy defect in CdTe for neutral charge state and chemical potential $\mu_{\text{cation}}=0$ are calculated as shown in the Fig. 4. The formation energy of Cd vacancy defect in CdTe is in good agreement with the previous results.³ The formation energy of the Hg vacancy defect in MCT has a nearly linear relationship with the mole fraction x . The formation energy becomes smaller as the mole frac-

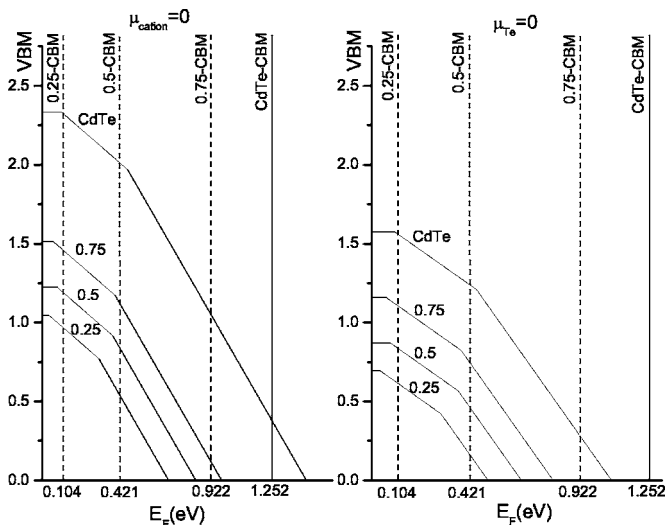


FIG. 5. The calculated formation energies of the Hg vacancy defect for MCT with $x=0.25, 0.5, 0.75$, and Cd vacancy defect for CdTe as a function of the Fermi levels. The VBM of all the four materials is set to zero.

tions of MCT are decreased. The result indicates that the Hg vacancy defects occur more easily as the mole fraction is decreased. Taking the atom as the reference, the formation energy of $\text{Hg}_{0.75}\text{Cd}_{0.25}\text{Te}$ is 1.72 eV, in good agreement with the experimental result.⁴ Figure 5 shows the calculated formation energies of Hg vacancy defects for MCT with $x=0.25, 0.5$, and 0.75 , and Cd vacancy defect for CdTe as a function of the Fermi energy. In the figure, the slope of the line gives the charge state of the defect at the Fermi energy. The transition energy level is the Fermi energy, at which the slope of the lines changes. Under the Hg- or Cd-rich condition, the chemical potential of μ_{Hg} or μ_{Cd} equals to zero. Under the Te-rich condition, the cation chemical potential becomes complicated due to the alloying effect. Here, we simply choose the formation energy of HgTe and CdTe. (The calculated formation energies of HgTe and CdTe are -0.35 eV and -0.76 eV, respectively. The results are in good agreement with the experimental values.³⁶⁻³⁸) as the cation chemical potential because our main motivation is the relation between the transition energy level and the mole fraction of MCT. The transition energy levels of V_{Cd} in CdTe are $\varepsilon(0/-1)=0.10$ eV and $\varepsilon(-1/-2)=0.43$ eV, respectively, in agreement with the previous results under the calculated error. The calculated results show that the transition energy level shifts to the deeper position within the band gap as the mole fraction becomes larger. The double acceptors caused by the cation vacancy defect are two empty states of t_{2v} , coming mainly from the p -like orbitals. The transition energy level moves more deeply into the band gap as the Cd mole fraction becomes larger which agree well with the experimental results.^{39,40} As shown in Fig. 5, either under the Hg-rich or Te-rich condition, for $x=0.25$ the transition energy level of $\varepsilon(0/-1)$ is 37 meV and the transition energy level of $\varepsilon(-1/-2)$ is 0.31 eV, which is larger than the calculated band gap (0.1 eV). By considering the calculated error bar in the transition energy levels, the $\varepsilon(0/-1)$ may locate in the band gap of the real MCT with $x=0.25$ and behave as a

shallow acceptor. However the $\varepsilon(-1/-2)$ is always larger than the band gap of MCT with $x=0.25$ (the real band gap about 0.15 eV). The results imply that the second ionization of the double acceptors merges in the direct band-to-band electronic transition process. Namely, the second order ionization of the double acceptors cannot occur in MCT with $x=0.25$. The experimental results indicate that the concentration of the acceptors is nearly equal to that of Hg vacancy defect around $x=0.2\sim 0.3$.⁴¹ The calculated transition energy levels and the results can be used to explain the experimental observations.

Here, we give a further discussion about the results. From our calculations, the transition energy levels for $\varepsilon(0/-1)$ of the mercury vacancy defect of MCT are all below 0.1 eV, meaning the Hg vacancy defect causes a shallow acceptor. The theoretical predications, especially the trend of the transition energy levels related to the mole fraction of MCT, are in good agreement with the experimental results.^{2,39,40} The theoretical results also indicate that the p -type MCT caused by native Hg vacancy defect becomes more efficient with the Cd mole fraction becoming smaller because the acceptor becomes shallower. Moreover, the transition energy levels for $\varepsilon(-1/-2)$ are all around 0.3 eV. By considering the calculated errors, the energy level can be seen as a trap center. The results are agreement with the experimental observation, in which a trap center around 0.15 eV (see Ref. 42) above the VBM occurs because of the Hg vacancy defects.

C. Bonding mechanism

To indicate the strength of orbital hybridization in the MCT materials, one can examine the density of states and its partial density of states (p -DOS), in which it is shown how the "atomic" levels evolve into the band states. The total and partial density of states are calculated using the modified tetrahedron integration method⁴³ and are broadened using a Gaussian-like function with full width at half-maximum being equal to 0.1 eV. The total density of states of $\text{Hg}_{0.5}\text{Cd}_{0.5}\text{Te}$ with and without a mercury vacancy are shown in Fig. 3. The main difference is that the valence bottom in the Fig. 3(b) has two DOS peaks around -10.2 eV. It is known that the valence band bottom of II-VI semiconductors comes from the anion s state. The double DOS peaks demonstrate that the energy level of some Te $5s$ states is split in the MCT with a mercury vacancy. By comparing the anion's partial DOS of different sites, it is found that the upshift of the $5s$ energy states comes mainly from the four NN Te atoms. Figure 6 shows the s partial DOSs of the NN tellurium and the seventh-nearest-neighbor tellurium. The NN Te $5s$ energy states shift upwards for about 0.55 eV relative to the Te $5s$ energy states of the other shell lattice site. Thus, the energy upshift of the Te $5s$ states is related with the NN Te dangling bond rehybridization. The valence charge density and the bonding charge density of the NN Te $5s$ states are calculated as shown in the Fig. 7. From Fig. 7(a), it is found that the charge density of Te $5s$ state closely distributes around the Te and the nearest-neighbor cations. For the perfect MCT with tetrahedral symmetry, each tellurium atom has four nearest-neighbor cations with delocalized $5s$

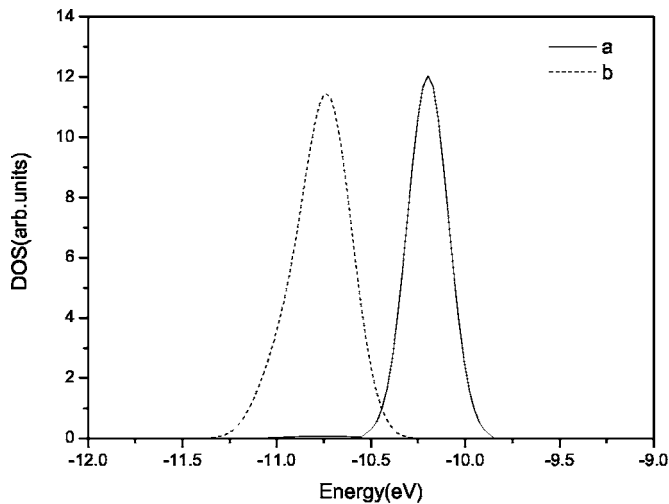


FIG. 6. The comparison between the nearest neighbor (NN) Te s p -DOS and the seventh-neighbor Te s p -DOS in the furthest from the vacancy. Solid line (a) is the result of the NN Te and the dash line (b) is the result of seventh-neighbor Te.

electrons. However, in the MCT with vacancy defect, the nearest-neighbor tellurium of the vacancy has three NN cations. The result decreases the distributing space of $5s$ electrons. The reduction of the distributing space of the NN Te $5s$ state electrons leads to the increase of charge concentration around the NN Te and NNN cations [as shown in Fig. 7(b)], and makes the kinetic energy of the NN Te $5s$ states higher than that of the other site Te atoms. Finally the reduction makes the energy of NN Te $5s$ states shift to higher energy. Moreover, the Te $5s$ electrons distribute mainly along the bond between NN Te and NNN cations. The contract relaxations of bond for NN Te and NNN cations, as

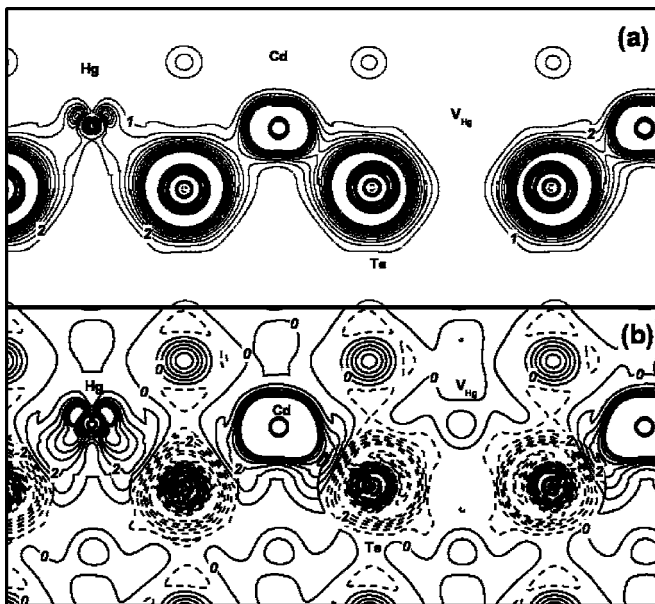


FIG. 7. Charge density (a) and the bonding charge density (b) of the Te $5s$ states. The contour step size is $2 \times 10^{-3} e/(\text{a.u.})^3$ for the total charge density (a) and $1 \times 10^{-3} e/(\text{a.u.})^3$ for the bonding charge density (b).

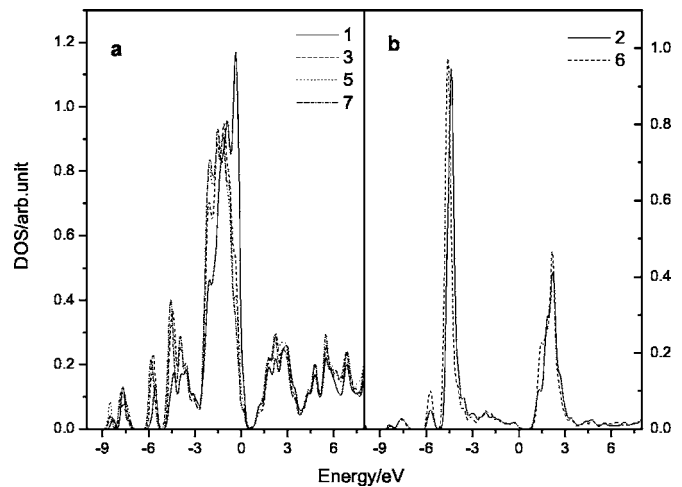


FIG. 8. The comparison of the Te- p states in different shell sites (a) and the comparison between the next-nearest-neighbor (NNN) Hg s p -DOS and the sixth-neighbor Hg s p -DOS in the furthest from the vacancy (b). The number in the (a) and (b) means the neighbor shell.

listed in Table I, also lead to upshift of the Te $5s$ energy. The upshift of Te $5s$ state energy is also observed for other mole fractions. We also checked the energy shift by using the PAW method with 64-, 256-, and 512-atom supercells. It is found that the energy upshift of Te $5s$ states is about 0.1–0.3 eV. The difference between the Te $5s$ energy shifts of FP-LAPW and PAW can be attributed to the neglect of SO coupling in PAW calculations.

Based on the same analysis as mentioned above, we can find that the dangling bond rehybridization induced by vacancy defect also has effect on the other electronic states of the material. We focus on the situation of the band edge states, namely, the valence band maximum (VBM) and the conduction band minimum (CBM) because the band gap of the materials is determined by them. It is known that the bands in the vicinity of the VBM and the CBM have strong Te p and cation- s characteristics for the II-VI semiconductors, respectively. The partial DOSs of Te $5p$ and cation- s states for different neighbor shell sites of $\text{Hg}_{0.5}\text{Cd}_{0.5}\text{Te}$ are calculated as shown in Fig. 8, in which only the Hg $6s$ states are shown. The figure indicates that the energy states of NN Te p in VBM around the defect move upwards as the Te $5s$ states, but the Hg s states in CBM nearly keep the same position at different shell sites. Further, it is demonstrated that the energy upshift of the electronic states mainly is caused by the NN Te dangling bond rehybridization. The defect and the dangling bond rehybridization mainly have effect on the nearest-neighbor shell. The effect becomes weaker as the neighbor shell is farther from the vacancy site. From the calculations, it is also found that the band gap becomes smaller due to the structural change. As mentioned above, the vacancy is created by removing two valence electrons from cation. The removing causes the dangling bond orbitals of two electrons around the vacancy so that the vacancy is a double acceptor with two levels at different ionization energies, just above the VBM. For the tetrahedral symmetry group, the defect states consist of a low-lying sin-

glet a_1^v state and a high-lying threefold-degenerate t_2^v states. For the case of charged neutral V_{Hg}^0 , the defect center has total six electrons. Two of them occupy the a_1^v state, while the remaining four electrons occupy the t_2^v states. In this way, there is one t_2^v unoccupied state just above the the VBM, acting as double acceptor. The acceptor levels determined by single-particle energy state are 106 and 135 meV above the VBM for $\text{Hg}_{0.5}\text{Cd}_{0.5}\text{Te}$, respectively. The first acceptor level calculated here agrees well with the experimental results³⁹ of the ionization energy of the mercury vacancy, and the second acceptor level locates in the position of the 42% band gap from the VBM. The calculated band gap of the $\text{Hg}_{0.5}\text{Cd}_{0.5}\text{Te}$ with mercury vacancy defect by FP-LAPW method is 320 meV, and the band gap is smaller than that of PAW method due to the SO coupling effects.⁴⁴ The total DOS (shown in Fig. 3) includes the two un-occupied single electron energy states above the VBM. Actually, the band gap of $\text{Hg}_{0.5}\text{Cd}_{0.5}\text{Te}$ with Hg vacancy defect is 90 meV larger than that of the pure materials from the calculation. As Wei *et al.*⁴⁵ have pointed out that the p - d coupling plays an important role in the II-VI semiconductor's VBM, behaving as the p - d repulsion. The magnitude of the repulsive coupling can be estimated quantitatively by considering the p - d repulsive energy perturbatively, as

$$\Delta E_{pd} \sim V_{pd}^2 / (\epsilon_p^a - \epsilon_d^c), \quad (3)$$

where the V_{pd}^2 is the coupling matrix element and $(\epsilon_p^a - \epsilon_d^c)$ is the atomic energy differences between the anions and cations. Because one cation is lost in the system, mercury vacancy defect reduces the p - d repulsive energy ΔE_{pd} . The effect induces the downshift of the energy of the NN Te p states. Finally, the upshifted Te p states in Fig. 6(a) are the empty t_2^v states, coming from the rehybridization of the NN Te dangling bond. Therefore, the empty states cause the response wavelength of MCT with Hg vacancy to become longer although the Hg vacancy widens the band gap. The above conclusions are also confirmed by the calculations for

other mole fractions and by PAW method with 256- and 512-atom supercells.

IV. CONCLUSION

By using the first-principles methods, the structural and electronic properties of a mercury vacancy defect in the $\text{Hg}_{1-x}\text{Cd}_x\text{Te}$ have been studied. The defect leads to inward relaxations and the reasons for the relaxations of NN tellurium have been revealed clearly by the analysis of the valence charge density and the bonding charge density. The inward relaxation is mainly determined by the negative charge accumulation. We found that the charged state of the systems enhances the relaxation. The formation energy and transition energy levels of the cation vacancy defects have been shown for different mole fractions. In combination with the analysis of the calculated acceptor levels induced by mercury vacancy, the predicated acceptor levels, especially the trend of the acceptor levels according to the mole fraction of MCT, are in good agreement with existing experimental results.^{35,39-42} Meanwhile, we also show that the rehybridization of the dangling bond of the NN Te atom around the mercury vacancy leads to upshift of the Te $5s$ states. In addition, the mercury vacancy defect increases the band gap in comparison with that of the pure materials due to the weaker p - d coupling, but the acceptor levels in the band gap make the response wavelength become longer for the MCT material with a mercury vacancy defect.

ACKNOWLEDGMENTS

The authors would like to thank Jijun Zhao for reading the paper. This work is supported in part by Chinese National Key Basic Research Special Fund, Key fund of Chinese National Science Foundation (10234040), Chinese National Science Foundation (60476040, 60576068), Grand Foundation of Shanghai Science and Technology (05DJ14003), and the computational support from Shanghai Super-computer Center.

*Electronic address: xschen@mail.sitp.ac.cn

†Electronic address: luwei@mail.sitp.ac.cn

- ¹N. Mainzer, E. Lakin, and E. Zolotoyabko, *Appl. Phys. Lett.* **81**, 763 (2002).
- ²C. E. Jones, K. James, J. Merz, R. Braunstein, M. Burd, M. Eetemadi, S. Hutton, and J. Drumheller, *J. Vac. Sci. Technol. A* **3**, 131 (1985).
- ³Su-huai Wei and S. B. Zhang, *Phys. Rev. B* **66**, 155211 (2002).
- ⁴H. R. Vydyanath, *J. Electrochem. Soc.* **128**, 2609 (1981).
- ⁵M. C. Gold and D. A. Nelson, *J. Vac. Sci. Technol. A* **4**, 2040 (1986).
- ⁶Y. Selamet, C. H. Grein, T. S. Lee, and S. Sivananthan, *J. Vac. Sci. Technol. B* **19**, 1488 (2001).
- ⁷V. Gopal and S. Gupta, *Appl. Phys. Lett.* **95**, 2467 (2004).
- ⁸M. A. Berding, M. van Schilfgaarde, and A. Sher, *MRS Symposium Proceedings No. 216* (Materials Research Society, Pittsburgh, 1991), p. 3.

- ⁹Mei-Fan Sung Tang and David A. Stevenson, *J. Vac. Sci. Technol. A* **7**, 544 (1989).
- ¹⁰M. Zandian, A. C. Chen, D. D. Ewall, J. G. Pasko, and J. M. Arias, *Appl. Phys. Lett.* **71**, 2815 (1997).
- ¹¹M. A. Berding *et al.*, *J. Electron. Mater.* **27**, 605 (1997).
- ¹²R. S. Stapp *et al.*, *Appl. Phys. Lett.* **52**, 1614 (1988).
- ¹³Amit Garg, Avinashi Kapoor, Kailash N. Tripathi, and Surendera K. Bansal, *Proc. SPIE* **5273**, 303 (2004).
- ¹⁴Myriam H. Aguirre, Horacio R. Cnepa, and Noem E. Walse de Reca, *J. Appl. Phys.* **92**, 5745 (2002).
- ¹⁵V. A. Cotton and J. A. Wilson, *J. Vac. Sci. Technol. A* **4**, 2177 (1986).
- ¹⁶J. T. Schick, and C. G. Morgan-Pond, *Semicond. Sci. Technol.* **5**, S81 (1990).
- ¹⁷M. A. Berding, M. van Schilfgaarde, and A. Sher, *Phys. Rev. B* **50**, 1519 (1994).
- ¹⁸M. A. Berding, *Phys. Rev. B* **60**, 8943 (1999).

- ¹⁹M. A. Berding, M. van Schilfgaarde, and A. Sher, *J. Vac. Sci. Technol. B* **B10**, 1417 (1992).
- ²⁰L. A. Errico, G. Fabricius, M. Renteria, P. dela Piesa, and M. Forker, *Phys. Rev. Lett.* **89**, 055503 (2002).
- ²¹L. A. Errico, G. Fabricius, and M. Renteria, *Phys. Rev. B* **67**, 144104 (2003).
- ²²P. Hohenberg and W. Kohn, *Phys. Rev.* **136**, B864 (1964); W. Kohn and L. J. Sham, *Phys. Rev.* **140**, A1133 (1965).
- ²³P. Blaha, K. Schwarz, G. Madsen, D. Kvasnicka, and J. Luitz, *WIEN2k, An Augmented Plane Wave + Local Orbitals Program for Calculating Crystal Properties* (Karlheinz Schwarz, Techn. University Wien, Austria, 2001).
- ²⁴J. P. Perdew, K. Burke, and M. Ernzerhof, *Phys. Rev. Lett.* **77**, 3865 (1996).
- ²⁵Bernd Kohler, Steffen Wilke, and Matthias Scheffler, *Comput. Phys. Commun.* **94**, 31 (1996).
- ²⁶R. Yu, D. Singh, and H. Krakauer, *Phys. Rev. B* **43**, 6411 (1991).
- ²⁷B. Kohler, S. Wilke, M. Scheffler, R. Kouba, and C. Ambrosch-Draxl, *Comput. Phys. Commun.* **94**, 31 (1996).
- ²⁸G. Kresse and J. Furthmuller, *Phys. Rev. B* **54**, 11169 (1996).
- ²⁹G. Kresse and J. Furthmuller, *Comput. Mater. Sci.* **6**, 15 (1996).
- ³⁰D. Vanderbilt, *Phys. Rev. B* **32**, 8412 (1985).
- ³¹S. B. Zhang and J. E. Northrup, *Phys. Rev. Lett.* **67**, 2339 (1991).
- ³²C. K. Shih and W. E. Spicer, *Phys. Rev. Lett.* **58**, 2594 (1987).
- ³³J. Lento, J.-L. Mozos, and R. M. Nieminen, *J. Phys.: Condens. Matter* **14**, 2637 (2002).
- ³⁴F. D. Murnaghan, *Proc. Natl. Acad. Sci. U.S.A.* **30**, 244 (1994).
- ³⁵M. A. Berding, A. Sher, and A.-B. Chen, *J. Vac. Sci. Technol. A* **5**, 3009 (1987).
- ³⁶C. Kittel, *Introduction to Solid State Physics*, 6th ed. (Wiley & Sons, New York, 1986).
- ³⁷W. A. Harrison, *Electronic Structure and the Properties of Solids* (Freeman, San Francisco, 1980).
- ³⁸*CRC Handbook of Chemistry and Physics*, 81st ed., edited by D. R. Lide (CRC Press, New York, 2000).
- ³⁹X. H. Shi, S. Rujirawat, R. Ashokan, C. H. Grein, and S. Sivananthan, *Appl. Phys. Lett.* **73**, 638 (1998).
- ⁴⁰A. T. Hunter and T. C. McGill, *J. Appl. Phys.* **52**, 5779 (1981); A. T. Hunter and T. C. McGill, *J. Vac. Sci. Technol.* **21**, 205 (1982).
- ⁴¹D. E. Copper and W. A. Harrison, *J. Vac. Sci. Technol. A* **8**, 1112 (1990).
- ⁴²D. L. Polla and C. E. Jones, *J. Appl. Phys.* **51**, 6233 (1980).
- ⁴³P. E. Blöchl, O. Jepsen, and O. K. Andersen, *Phys. Rev. B* **49**, 16223 (1994).
- ⁴⁴C. S. Wang and B. M. Klein, *Phys. Rev. B* **24**, 3393 (1981).
- ⁴⁵Su-Huai Wei and Alex Zunger, *Phys. Rev. B* **37**, 8958 (1988).